Exosomes from young healthy human plasma promote functional recovery from intracerebral hemorrhage via counteracting ferroptotic injury

Wenqin Yang [a,b,1], Ning Ding [a,1], Ran Luo [a,1], Qian Zhang [c], Zhenhua Li [d], Fengchun Zhao [a], Shuixian Zhang [a], Xuyang Zhang [a], Tengyuan Zhou [a], Haomiao Wang [a], Long Wang [a], Shengli Hu [a], Guixue Wang [e,f], Hua Feng [a], Rong Hu [a,f,*]

[a] Department of Neurosurgery, Key Laboratory of Neurotrauma, Southwest Hospital, Third Military Medical University (Army Medical University), 400038, Chongqing, China
[b] Bioengineering College of Chongqing University, Chongqing, 400030, China
[c] Medical Research Center, Southwest Hospital, Third Military Medical University (Army Medical University), 400038, Chongqing, China
[d] Affiliated Dongguan Hospital, Southern Medical University, Dongguan, 523059, China
[e] Key Laboratory of Biorheological and Technology of Ministry of Education, State and Local Joint Engineering Laboratory for Vascular Implants, Bioengineering College of Chongqing University, Chongqing, 400030, China
[f] JinFeng Laboratory, Chongqing, 401329, China

ARTICLE INFO

ABSTRACT

Intracerebral hemorrhage (ICH), as a type of life-threatening and highly disabled disease, has limited therapeutic approaches. Here, we show that exosomes derived from young healthy human plasma exhibiting typical exosomes features could facilitate functional recovery of ICH mice. When these exosomes are intraventricularly delivered into the brain after ICH, they mainly distribute around the hematoma and could be internalized by neuronal cells. Strikingly, exosomes administration markedly enhanced the behavioral recovery of ICH mice through reducing brain injury and cell ferroptosis. MiRNA sequencing revealed that microRNA-25-3p (miR-25-3p) was differentially expressed miRNA in the exosomes from young healthy human plasma, compared with exosomes from the old control. Importantly, miR-25-3p mimicked the treatment effect of exosomes on behavioral improvement, and mediated the neuroprotective effect of exosomes against ferroptosis in ICH. Furthermore, luciferase assay and western blotting data illustrated that P53 as assumed the role of a downstream effector of miR-25-3p, thereby regulating SLC7A11/GPX4 pathway to counteract ferroptosis. Taken together, these findings firstly reveal that exosomes from young healthy human plasma improve functional recovery through counteracting ferroptotic injury by regulating P53/SLC7A11/GPX4 axis after ICH. Given the easy availability of plasma exosomes, our study provides a potent therapeutic strategy for ICH patients with quick clinical translation in the near future.

1. Introduction

Intracerebral hemorrhage (ICH), a serious disease that threatens life, accounts for 15–20% of strokes [1], and most survivors suffer from life-long disability [2,3]. Pathological bases contributing to the poor prognosis of ICH are primary and secondary brain injury (SBI) [2], among which SBI is characterized by a complex range of pathologies, such as oxidative stress, inflammation, and apoptosis [4]. Ferroptosis, a newly found process of cell death, is different from other cell death modes [5], with a vital role in various brain diseases, including neurodegenerative diseases [6,7]. One of its characteristics is reactive oxygen species (ROS) accumulation and lipid peroxidation [8]. Especially in ICH, ferrous iron from hematoma degradation contributes to ROS accumulation from Fenton reaction, while ferrous also works as a prosthetic group of lipoperoxidase [9]. Therefore, ROS accumulation and iron deposition are easy to induce ferroptosis after ICH [10]. Indeed,

---

recent studies also suggest that ferroptosis in peri-hematoma site plays a crucial role in the SBI after ICH [11]. Thus, strategies that specially inhibit ferroptosis after ICH would be more promising.

Exosomes, a kind of cell derived small vesicle with the diameter of 50–150 nm, possesses the capacities of delivering nutrition and RNA sequences among different kinds of cells [12–14]. Studies have shown that exosomes from mesenchymal stem cells, neural stem cells, astrocytes, and microglia [15–17] could preserve neurocytes from many insults such as ICH via different pathways [18]. However, whether exosomes could protect neurocytes from ferroptosis remains unclear [19].

Exosomes are present in the circulation and their yield in plasma (or serum) was greatly higher than those secreted by a single cellular type [20,21]. Previously, convalescent plasma therapy has become an attractive treatment strategy for infectious and immunological diseases [22]. Traditionally, plasma therapy is believed to provide antibodies and nutrition to patients. Recently, studies have revealed that blood derived exosomes have lots of therapeutic effects [21], especially from young healthy plasma, which has been reported to be promising for treating inflammation [23] and COVID-19 [24]. However, the effect of exosomes from young healthy plasma on stroke (especially ICH) and its underlying mechanisms remain largely unknown.

Here, exosomes derived young healthy human plasma were delivered to ICH mice through intraventricular injection. Behavioral and molecular assays indicate that exosomes prevent cell ferroptosis from ICH and thereby improve functional recovery through miR-25-3p/P53/SLC7A11/GPX4 pathway. As far as we know, our study is the first to reveal that exosomes from healthy young human could inhibit ferroptotic injury after ICH and provide a new treatment approach.

2. Materials and methods

2.1. Young healthy human plasma collection

The corresponding peripheral blood samples were taken from 5 healthy young people aged 18–25 years and 5 healthy elderly people aged 65–70 years. The blood collection was approved by the Ethics Committee of Southwest Hospital of Third Military Medical University (AKY2022128), and each participant provided informed consent. Blood samples were placed in an EDTA anticoagulant tube, gently mixed, and centrifuged at 2500 g for 15 min at 4 °C, and the supernatant was taken. The supernatant was centrifuged again at 2500 g for 15 min, and the supernatant plasma was taken and kept at −80 °C for later application.

2.2. Exosomes characterizations

Freshly thawed plasma (2 mL) was centrifuged at 2000 g for 10 min and 12,000 g for 30 min at 4 °C to remove cell debris and larger vesicles, and was then filtered with a 0.22 μm syringe filter (SLGPO33RB, Millipore, UA). The filter was washed with 3 mL PBS (diluted to reduce viscosity). The diluted plasma was ultra-centrifuged at 120,000 g for 2 h at 4 °C. The precipitate was resuspended in 100 μL PBS to obtain exosomes solution. Transmission electron microscopy (TEM, JEM-1400FLASH, JEOL, Japan) was employed to identify exosomes forms. Nanoparticle tracking analysis (NTA, ZetasizerNanoZSP, US) was adopted for measurement of diameter and exosome concentration. The protein content was determined by BCA protein assay (P0011, Beyotime, Shanghai, China), and exosomes markers [25]. Western blotting analysis was used to for detecting CD9, CD63, CD81 and tumor susceptibility gene 101 (TSG101). Fluorescence labeling exosomes were synthesized using the DiD kit (C1039, Beyotime, Shanghai, China). In brief, DiD dye was incubated in the appeal resuspension for 10 min for exosomes staining. The dye in the solution was then removed by centrifugation of 100,000 g at 4 °C for 2 h. After centrifugation at 100,000 g for 2 h, the precipitate was rinsed using PBS to give dye-stained exosomes.

2.3. Mice ICH model

All experimental procedures were under the supervision of the Ethics Committee of the Southwest Hospital, Third Military Medical University, and complied with the guidelines of the National Institutes of Health Guide for the Care and Use of Laboratory Animals (approval no. AMUWEC20224040). ICH autologous blood injection model. Mice were first anesthetized with a 2% isoflurane/air mixture [26]. Then the anterior fontanelle and posterior fontanelle were exposed. A hole was drilled at 0.8 mm in front of the anterior fontanelle and 2 mm lateral to the midline. The tails of mice were disinfected with 75% alcohol and 25 μL of autologous blood was collected in the tails of mice with a micro syringe (Hamilton, Romania) and slowly injected into the basal ganglia as deep as 3.5 mm with a 2 μL/min rate. For the sham mice, we performed the same operation but injected the same volume of saline. During operation, the body temperature of the mice was maintained at 37 °C ± 0.3 °C with a constant temperature heating plate until the mice woke up. The operation was performed by skilled researchers to minimize pain or pain during the experiment. After surgery, the mice were allowed to obtain food and water freely under constant photoperiod (12-h light/dark cycle), temperature (22–25 °C) and water (55–60%).

2.4. Animal experimental design

In total, 180 adult C57BL/6 mice (male, 24–26 g, 9–10 weeks, 168 were included in experiments and 12 did not survive during experiments) were used in the study. This study included seven parts (Fig. 1E). In the first part, DiD-labeled exosomes were injected into the lateral ventricle, and tissues were collected after 1 day for immunostaining. In the second part, after ICH, exosomes of different doses were injected into the lateral ventricle for three consecutive days. The mice received behavioral tests on days 1,3,7,14, and 28, and then the mice were euthanized. In the third part, after ICH, 40 μg exosomes were injected into the lateral ventricle for three consecutive days. On day 7, tissue was collected for immunostaining, Nissl staining, HE staining, and TEM detection. In the fourth part, RNA sequencing of plasma exosomes from young and elderly people was performed. Elder plasma exosomes were injected into the lateral ventricle for three consecutive days. Behavioral tests were carried out on days 1, 3, 7, 14, and 28, and mice were euthanized. In the fifth part, we injected miR25-3p of different doses into the lateral ventricle for three consecutive days, behavioral tests were carried out in mice on days 1,3,7,14, and 28, and euthanasia was performed on mice. In the sixth part of this study, 40 μg exosomes and 2 μM miR25-3p were injected into the lateral ventricle for three consecutive days. On day 7, the tissues were collected for Western blotting, PCR, MDA, GSH and immunostaining.

2.5. Behavioral tests

2.5.1. Open field test

The open field test (OFT) [27] was carried out for assessing overall locomotion of mice. The open field used an open three-dimensional space with a length of 50 cm × width of 50 cm × height of 50 cm. The mice were put in the open field, were able to move without restriction for 5 min, and the video was recorded. Then we cleaned up the smell left by the previous mouse and put it into the next mouse for experiment. The data analysis was carried out by two independent testers and software (ViewPoint behavioral technology, Lyon, France) was used for measuring the distance of the entire free movement.

2.5.2. Beam walking test

The beam walking test (BWT) [28] was carried out for the measurement of the motor coordination of mice after ICH. In brief, a 100 cm long and 1 cm wide wooden beam was erected 50 cm from the ground, and cotton was laid on the ground to prevent mice from falling. The mice were trained 3 days before ICH surgery to walk from one side of the
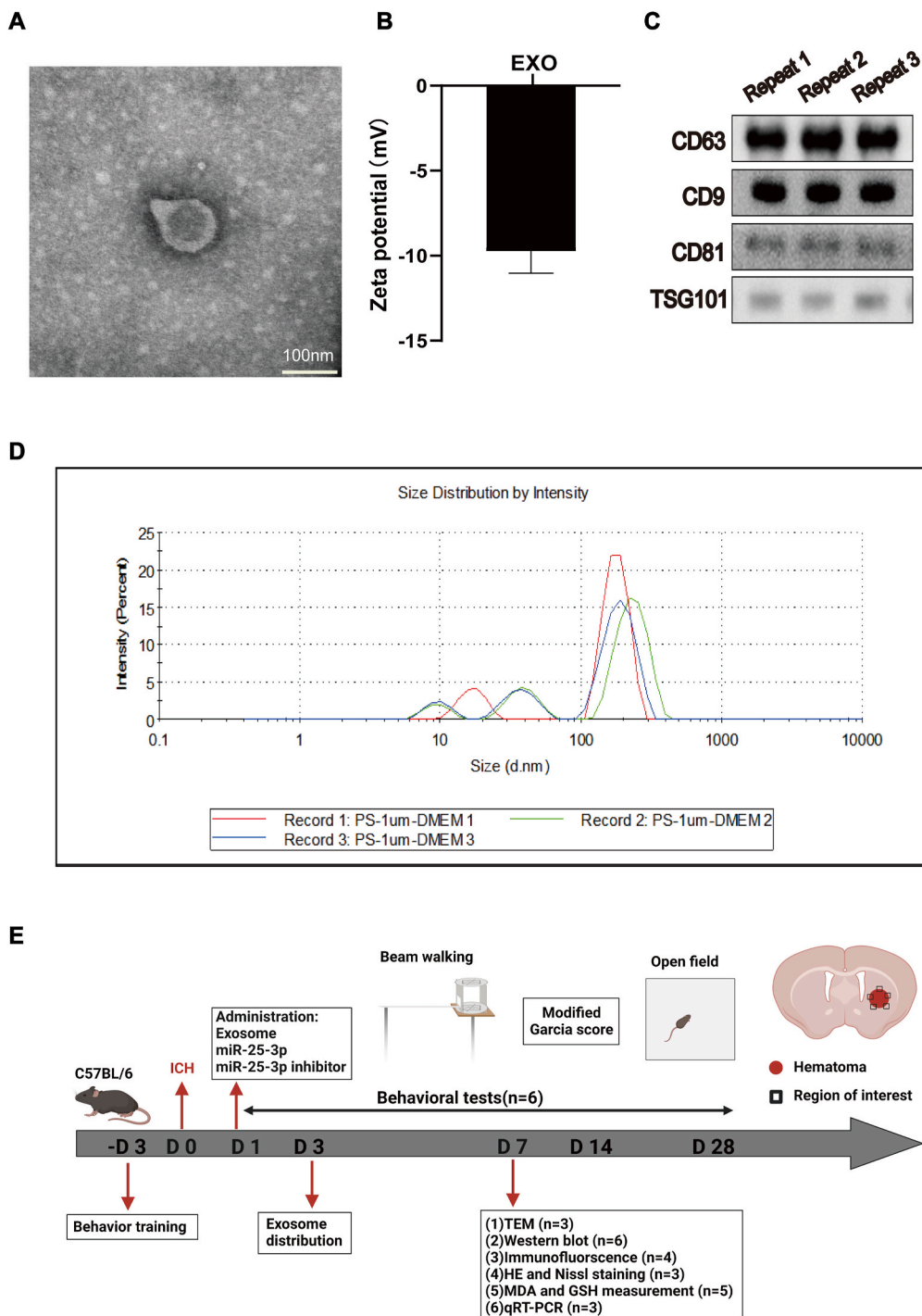
Fig. 1. Characterization of exosomes from young healthy man plasma.

(A) Transmission electron microscopy imaging of young human plasma-derived exosomes (Scale bars = 100 nm). (B) Zeta potential of young human plasma-derived exosomes. (C) Expression of exosomal markers CD63 , CD9, CD81 and TSG101 in young human plasma-derived exosomes. (D) Particle size distribution of young human plasma-derived exosomes measured by DLS analysis. (E) Experiment design and timeline. Behavior training was started 3 days before ICH. Baseline information was collected 1 day before ICH. Behavioral tests (Open field, Beam-walking and Modified Garcia Score) were conducted on days 1, 3, 7, 14 and 28. DiD-labeled exosomes were injected for immunostaining to evaluate the distribution and uptake of exosomes in the ICH brain. Then, exosomes, miR-25-3p and miR-25-3p inhibitors were injected on the first day after ICH in mice. Immunofluorescence staining, transmission electron microscopy, immunoblotting, qRT-PCR, MDA and GSH were performed on the 7th day to assess ferroptosis after ICH. HE and Nissl staining were performed to assess tissue and cell injury after ICH. The red rectangle indicates the location of the hematoma, and the black rectangle indicates the area used for experimental sampling.

beam to the other side until they could overcome the fear of heights and pass smoothly. After surgery, each mouse passed the beam three times under video recording. Then, two independent examiners who were unaware of the experimental group calculated the slip ratio of the contralateral limbs during the entire three walks from the video.

2.5.3. Modified Garcia score

Gross motor function was evaluated using the modified Garcia behavior score [29]. It is a comprehensive assessment of the scores of motor, reflex and balance tests after ICH in mice. The severity score was 0–21 points, of which 21 points represent normal, and the lower the score, the more serious the injury. The experiment was evaluated by a researcher unaware of the experimental design before and after ICH in mice.

2.6. Transmission electron microscopy (TEM)

TEM was adopted for observation of the ultrastructure of mitochondria from different groups. In short, after the end of perfusion, about 1 mm^3 of brain tissue around the hematoma was immediately placed in 3% glutaraldehyde fixative, fixed at 4 °C for 10 h, and rinsed with PBS for three times. Subsequently, acetone was dehydrated step by step, resin embedding and polymerization, ultra-thin sections of 60–80 nm (EM UC7, Leica) were made and placed on a 300mesh nickel mesh. A

layer of parafilm was attached to the staining plate in the staining wet box, and 3% hydrogen peroxide was dropped on the parafilm to form water droplets. The sliced nickel mesh was etched downward on the water droplets for 30 min, and then was washed using double distilled water and PBS for 5 times. After this, it was incubated with 1% calf serum at room temperature for 20 min. Following the removal of the calf serum, the first antibody was incubated at 4 °C for 20 h, washed with PBS for 5 times, and then incubated with 1% calf serum at room temperature for 20 min. The calf serum was sucked out. Next, the second antibody labeled with colloidal gold was incubated at room temperature for 2 h and washed with PBS for 5 times. Finally with uranyl acetate, lead citrate mild counterstaining, double distilled water washed 5 times, natural drying, electron microscopy (Hitachi HT7700, Japan) was used to observe these samples.

2.7. H&E and nissl staining

The brain tissue was first perfused with 0.9% normal saline, fixed with 4% paraformaldehyde, and finally dehydrated using 30% sucrose solution prepared with 0.01 M PBS for two days. We serially sliced (5 μm) the brain slices with a cryostat microtome (CM1860UV, Wetzlar, Germany), and stained coronal sections with 0.1% cresyl violet (Nissl) or hematoxylin and eosin (H&E) [30], and finally mounted with neutral resin. The samples were studied through an image processing software (Case viewer, 3DHISTEC, Budapest, Hungary). Then the hematoma size was quantified by software.

2.8. GSH and MDA analyses

MDA and GSH assays were performed using MDA and GSH kits (A020–2, A003-1-2, Jian Cheng, Nanjing, China). Briefly, ipsilateral brain tissue around the hematoma on day 7 was collected, lysed, and centrifuged, the working solution was added, and OD values were measured with a spectrophotometer (Varioskan Flash, Thermo Scientific, Walsam, MA, USA). By fitting a standard curve, MDA and GSH levels were calculated.

2.9. Immunostaining

The brain tissue was first perfused with 0.9% normal saline, fixed with 4% paraformaldehyde, and finally dehydrated with 30% sucrose solution prepared with 0.01 M PBS for two days. The brain slices were serially sliced (30 μm) with a cryostat microtome (CM1860UV, Wetzlar, Germany). The brain slices were blocked (0.5% Triton for 30min, 5% BSA for 2 h) and incubated in the presence of the following primary antibodies: Rb anti-GPX4 (1:500, Cat:52,455, Cell Signaling Technology, MA, USA); Ms anti-NeuN (1:200, Cat: 94,403, Abcam, Cambridge, UK); Ms anti-GFAP (1:500, Cat: 3670, Cell Signaling Technology, MA, USA); Rb anti-Iba-1 (1:200, Cat: 17,198, Cell Signaling Technology, MA, USA). Further, the antibodies were washed with PBS for 3 times with at least 3 min each and were administrated at room temperature for 2 h: Goat anti MS H&L 488 (1:500, Cat: ab150113, Abcam, Cambridge, UK); Goat anti Rb H&L 488 (1:500, Cat: ab150077, Abcam, Cambridge, UK). After washing with 0.01 M PBS, DAPI was stained in dark at room temperature for 10 min, and finally sealed with an anti-fluorescence quenching tablet (P0126, Beyotime, Shanghai, China). Photographing was performed using the confocal microscope (LSM 880, Carl Zeiss, Weimar, Germany). The image analysis was performed using Image J (Image J 1.8, NIH, USA).

2.10. Western blotting

Mouse brain tissue on day 7 post-ICH was obtained from salt perfusion. Peri-hematoma site was obtained through homogenate centrifugation at 4 °C, 12,000 rpm for 30 min. The protein concentration was determined using a Bicinchoninic Acid (BCA) method (Beyotime,

Shanghai, China) before it was mixed with loading buffer (Zen-bio, Chengdu, China). A total of 30 μg protein was separated by 10% or 12.5% SDS-PAGE under 80V electrophoresis and electro-blotted to polyvinylidene difluoride (PVDF, Roche, IN, USA) membranes. Then, the incubation of membranes was performed in 10% non-fat dry milk (Beyotime, Shanghai, China) in PBS at room temperature for 2 h. After that, the following primary antibodies were independently incubated under 4 °C overnight: Rb anti-GPX4 (1:1000, Cat : 52,455, Cell Signaling Technology, MA, USA); Rb anti-SLC7A11 (1:1000, Cat:12,691, Cell Signaling Technology, MA, USA); Rb anti-P53 (1:1000, Cat: A5761, ABclonal, Wuhan, China); Rb anti-CD63 (1:1000, Cat: ab134045, Abcam, Cambridge, UK); Rb anti-CD81 (1:1000, Cat:109,201, Abcam, Cambridge, UK); Rb anti-CD9 (1:1000, Cat: A19027, ABclonal, Wuhan, China); Rb anti-TSG101 (1:1000, Cat: A5789, ABclonal, Wuhan, China). Then, after PVDF membrane was washed using TBST for three times, it was immersed in the relevant secondary antibody (1:10,000, Wuhan Boster, China) and incubated for 2 h at room temperature. The optical density was presented via an imaging system (Evolution-Capt Edge, Vilber, France) and an immunoblotting chemiluminescence kit (Thermo Fisher Scientific, Walsam, MA, USA). Images are studied with the imaging system (Evolution-Capt Edge, Vilber, France).

2.11. Real-time fluorescence quantitative polymerase chain reaction

Total RNA was obtained from ICH mice on day 7 after anesthesia, and mice brain on injury site was obtained by transcardiac perfusion. Then the trizol reagent (Tiangen, Beijing, China) was used for RNA extraction following product manual. The RNA was reverse-transcribed into cDNA using a reverse transcription kit (Takara Bio Inc., Shiga, Japan) and then subjected to real-time quantitative-polymerase chain reaction (qRT-PCR) with a real-time fluorescent quantitative PCR instrument (Bio-Rad, Hercules, CA, USA) using SYBR-green Premix Ex TaqTM (Takara Bio Inc., Shiga, Japan). The reaction system of 25 μL (12.5 μL premix Taq, 8.5 μL RNAase-free water, 2 μL primers, 2 μL cDNA) was added to each well of the 96-well plate, and detection of each sample was performed for three times. Threshold cycle (CT) readings were obtained, and the relative expression of target gene mRNA underwent calculation using $2\text{-}\Delta\Delta CT$ method and normalization to glyceraldehyde-3-phosphate dehydrogenase (GAPDH) level in all samples was performed. The related expression was normalized to sham group.

Gene	Forward (5′–3′)	Reverse (5′–3′)
SLC7A11	TCTCCAAAGGAGGTTACCTGC	AGACTCCCCTCAGTAAAGTGAC
GPX4	GAGGCAAGACCGAAGTAAACTAC	CCGAACTGGTTACACGGGAA
GAPDH	CCAATGTGTCCGTCGTGGATCT	GTTGAAGTCGCAGGAGACAACC

The prime used were list below:

2.12. miR-25-3p and miR-25-3p inhibitor administration

miR-25-3p inhibitors and negative control (NC) were synthesized by GenePharma (Shanghai GenePharma, Shanghai, China). The sequence of miR-25-3p was 5′-CAUUGCACUUGUCUCGGUCUGA-3′, 3′-AGACC-GAGACAAGUGCAAUGUU-5'. MiR-25-3p was directly injected into the lateral ventricle after intracerebral hemorrhage. The miR-25-3p inhibitor sequence was 5′-UCAGACCGACAAGUGCAAUG-3′, and 40 μg EXO and 2 μM miR-25-3p inhibitor were mixed and injected into the lateral ventricle of mice after ICH.

2.13. Luciferase reporter assay

We performed luciferase activity assays based on previous report [31]. We assayed luciferase activity via the Dual-Luciferase® Reporter Assay System (YEASEN, Shanghai, China), and calculated the ratio of Renilla luciferase to firefly luciferase activity. The reporter gene vector

was transfected into 293T cells, and then the firefly luciferase reaction working solution and Renilla luciferase reaction solution were prepared and incubated at room temperature. A total of 20 μL cell lysate was taken, 100 μL firefly luciferase reaction solution was added, and the shake plate was mixed to determine the activity of firefly luciferase. A total of 100 μL of Renilla luciferase reaction solution was added, and the shake plate was mixed. After standing for 10 min, the activity of Renilla luciferase was detected. The results were expressed as firefly luciferase detection value/Renilla luciferase detection value.

2.14. Statistical analysis

All statistical analyses were performed using SPSS 18.0 software (SPSS, Inc., Chicago, USA). For group comparison, the two-tailed independent Student's t-test was used. To compare more than three groups, one-way analysis of variance (ANOVA) and Tukey 's post-hoc test were used. All statistical graphs were created with Graph Pad Prism 8.0. Unless otherwise stated, data are expressed as mean values in SEM. $P < 0.05$ was considered statistically significant.

3. Results

3.1. Extraction and identification of exosomes from the plasma of young healthy human

To obtain exosomes from healthy young man, we took the plasma from young volunteers to centrifuge at ultrahigh speed. Identification of exosomes was performed by Western blot, zeta analysis and transmission electron microscopy (Fig. 1A–C). Nanoparticle tracking analysis (NTA) showed that the obtained exosomes have a mean diameter of 110 nm (100–150 nm. Fig. 1D) and a negative zeta potential of −9.74 mV (Fig. 1B). The detection of CD63, CD9, CD81 and TSG101 expressions (exosomal surface markers) was conducted using Western blot analysis (Fig. 1C). The above data demonstrated that exosomes from young healthy man were successfully extracted and exhibited typical exosomes features.

3.2. Exosomes distribution and internalization in the hemorrhagic brain

To evaluate the therapeutic effect of exosomes from young man plasma on ICH mice, we first studied the biodistribution of exosomes after administration. Exosomes were first stained with DiD and then intraventricularly injected into the brain. Surprisingly, we found most of the exosomes accumulated primarily in the area adjacent to hematoma in the hemorrhagic brain while no obvious positive signal was detected in the sham brain except the wall of ventricle (Fig. 2A). Next, to determine which type of neural cells would internalize the exosomes, various kinds of cell types were specifically immunofluorescently labeled. Data showed that exosomes were predominantly internalized by neurons and microglia around the hematoma [32,33], while few colocalization was found in GFAP positive cells (Fig. 2B).

3.3. Exosomes from young healthy man plasma enhance locomotion recovery of ICH mice

To examine the therapeutic effect of exosomes from young man plasma on ICH, we established a mouse model of ICH with autologous blood injection (Figs. S1A and S1B). Several behavioral tests were taken to evaluate the overall behavior performance of mice in different groups. Compared with sham group, mice in ICH group showed markedly impaired motor function at each time point (day 1, day 3, day 7, day 14, day 28 after ICH, Fig. 3). Interestingly, intraventricular injection of exosomes with different concentrations (20, 40, 60 μg) promoted locomotion recovery of mice with ICH (Fig. S2), whereas the saline vehicle treatment produced no effect on functional recovery of ICH mice. The overall behavioral performance showed that middle dosage (40 μg) held

the best effect, while other dosages also showed effectiveness (Figs. S2B–D). Thus, middle dosage (40 μg) was selected for the following experiments.

3.4. Exosomes from young healthy man plasma reduce brain injury and cell ferroptosis after ICH

To elucidate the pathological base underlying the therapeutic effect of exosomes on ICH, Hematoxylin eosin (H&E) and Nissl staining of brain sections were performed. H&E staining (Fig. 4A) did not show damage in the sham group, while cells and extracellular matrix around the injury zone were disorganized after ICH or ICH + saline Vehicle. It was also observed that ICH + EXO (exosomes) group significantly ameliorated the neuronal disorganization and increased the cell number in the brain tissue. Furthermore, based on Nissl staining, we found that the number of Nissl bodies dropped significantly, neuronal morphology was disturbed, and neuronal staining intensity was significantly lower in the ICH or ICH + Vehicle groups than in the sham group. In contrast, the number of Nissl bodies grew with improvement of morphology in the ICH + EXO group, and significantly more intense staining was observed (Fig. 4B and C).

Recent evidence has indicated that ferroptosis plays a key role in the secondary injury after ICH. To examine whether exosomes exert neuroprotective effect via inhibiting ferroptosis, we performed immunofluorescent staining of GPX4, a crucial upstream negative regulator of ferroptosis [34], among different groups. As shown in Fig. 4D and E, the intensity of GPX4 was dramatically diminished in the ICH group in contrast to the sham group, whereas the exosomes robustly suppressed the reduction of GPX4 intensity. Moreover, transmission electron microscopic assay was executed for observing the mitochondria morphology, which showed that the percentage of shrunken or rounding mitochondria was greatly increased in ICH group (Fig. 4F), while the addition of exosomes prominently downregulated the percentage around hematoma in ICH + EXO group (Fig. 4F). Together, these data suggest that exosomes from young healthy man extenuate brain injury and cell death in ICH mice through counteracting ferroptosis.

3.5. Micro-RNA 25-3p is an active molecule inside exosomes from young healthy man plasma promoting locomotion recovery of ICH mice

Exosomes are known to transfer various bioactive molecules, such as microRNAs (miRNAs), to recipient cells. To dissect the molecular basis for the neuroprotective effect of exosomes, RNA sequencing was employed in this study. Meanwhile, to effectively identify the likely active microRNA, we isolated exosomes from the plasma of old people as control, which was tested to be ineffective for behavioral recovery of ICH mice (Fig. S3). We compared the miRNA profiling of exosomes from young man and old controls. According to the profiling results, exosomes-associated miRNAs with significant differences between young and old ones were screened. We found that miR-25-3p was stably different between exosomes from young man and old controls (Fig. 5A). The pathway analysis of differential expressed transcripts gave significant hits on many signaling pathways, such as P53 [35], cGMP-PKG, Ras, PI3K-Akt [36], etc (Fig. 5B).

To test whether miR-25-3p exerts similar effect of exosomes of young healthy man on functional recovery of ICH mice, the same behavioral tests were applied to miR-25-3p treated mice. To determine the optimal dose for ICH, dose response assay of miR-25-3p was carried out, which revealed that middle concentration (2 μM) of miR-25-3p treatment displayed best performance (Fig. S4). Intriguingly, miR-25-3p treatment presented similar effect to exosomes on behavioral recovery of ICH mice, which included incremental locomotion distance in open field (Fig. 5C and F), less foot-false in beam walking test (Fig. 5D), and higher score in the Modified Garcia score (Fig. 5E).
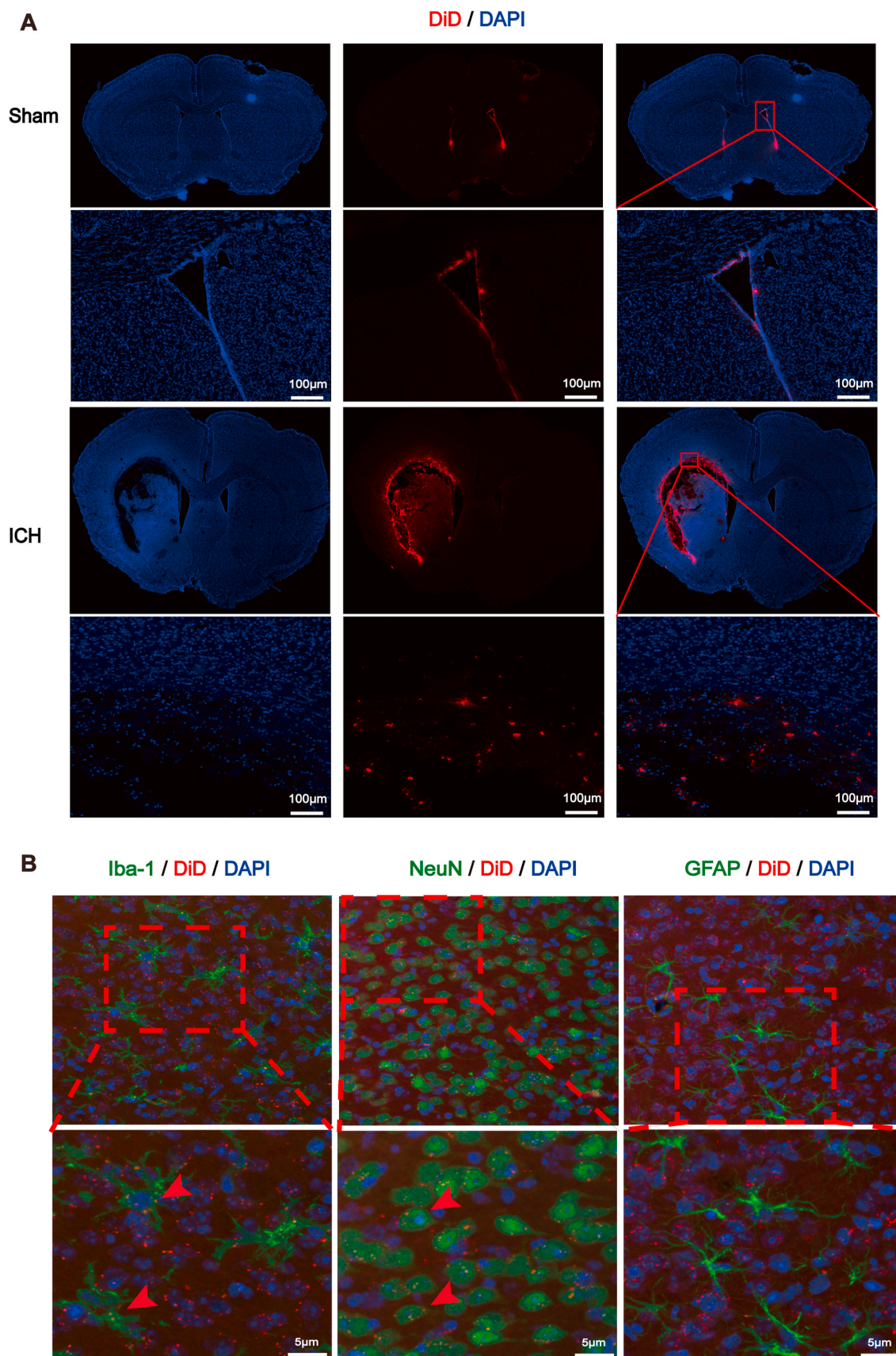
Fig. 2. Distribution and absorption of young plasma-derived exosomes in mouse brain after ICH.
(A) Confocal images showing the distribution of DiD-labeled exosomes *in vivo* in sham mouse brain and ICH mouse brain (Scale bars = 1000 μm). (B) Confocal photographs showing that DiD-labeled exosomes were uptaken by *in vivo* neurons and microglias, but not by astrocytes (Scale bars = 5 μm, n = 3 animals for each group).
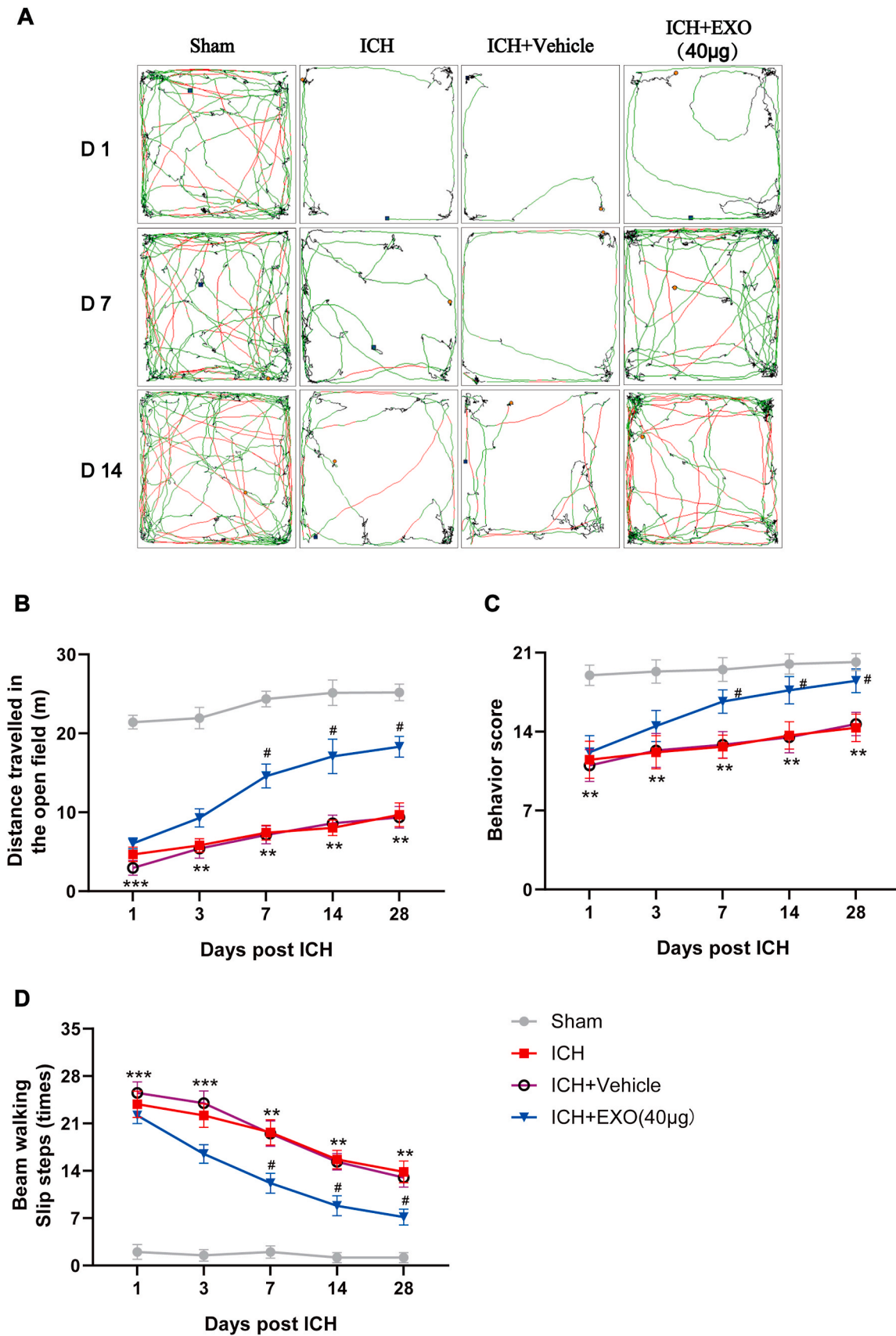
Fig. 3. Young human plasma-derived exosomes improve functional recovery of ICH mice.
(A) Representative open field movement trajectory of mice in different groups. (B) Summary data showing the distance travelled in the open field from experiment (A). (C) Gross motor function was evaluated using the modified Garcia behavior score. (D) Beam-walking test showing the slip ratio of the contralateral limbs in different groups. n = 6 animals for each group, **p < 0.01, ***p < 0.001 for ICH vs. sham; #p < 0.05 for ICH + EXO (40 µg) vs. ICH + Vehicle.
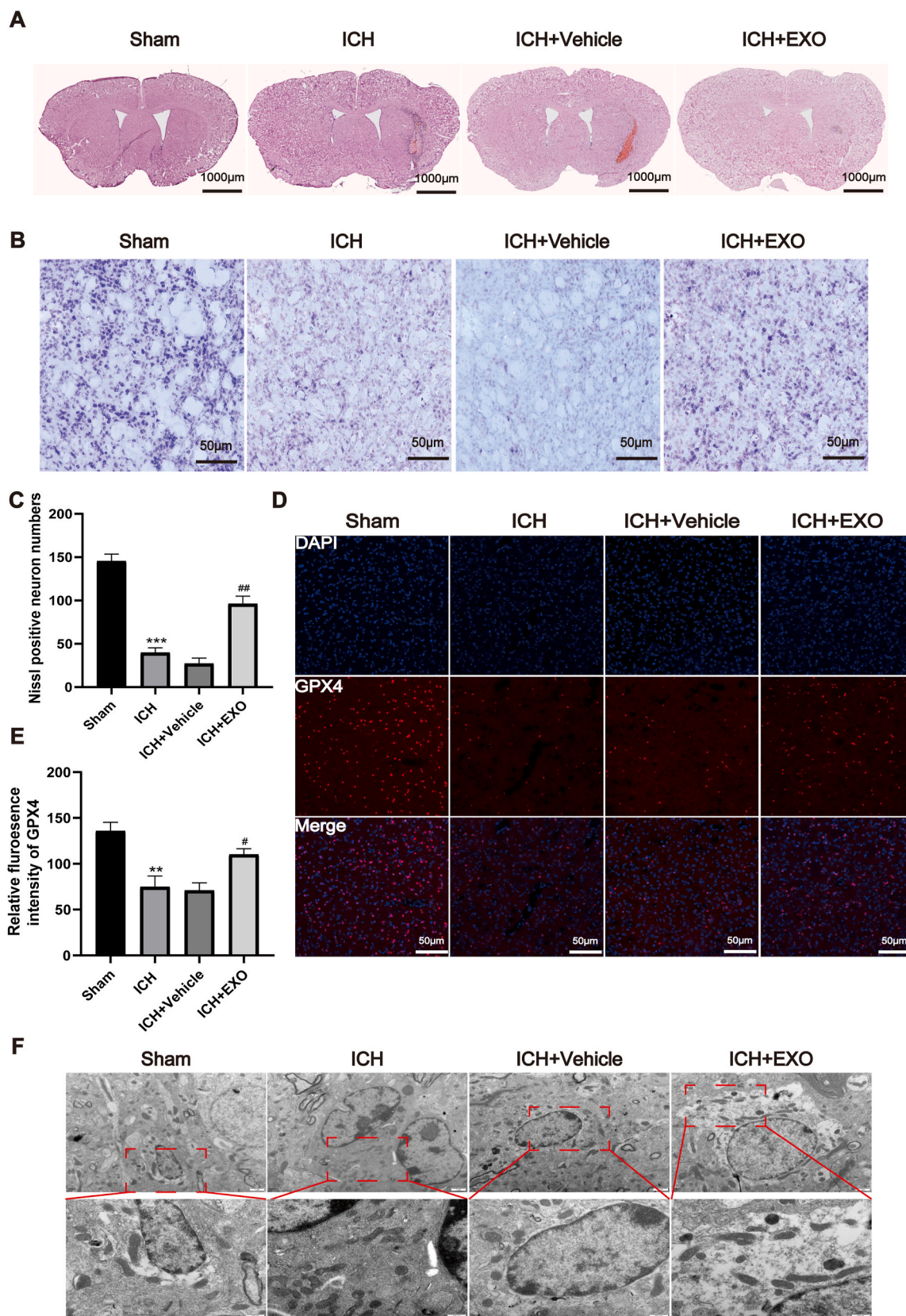
Fig. 4. Young human plasma-derived exosomes reduce brain injury and cell ferroptosis after ICH.
(A) HE staining images showing the gross damage of the mouse brain from Sham, ICH and EXO administered groups. (B) Representative photomicrographs of Nissl staining from different groups. (C) Quantification of Nissl-positive neurons in experiment (B) (n = 3 animals for each group). (D) Representative immunofluorescent images of GPX4 around hematoma from different groups. (E) Quantitative analysis of GPX4 staining (Scale bars = 50 μm, n = 4 animals for each group). (F) Transmission electron microscopy images showing the changes of mitochondria from different groups. Scale bars = 500 nm, n = 3 animals for each group, $**p < 0.01$, $***p < 0.001$ for ICH vs. sham; $^{#}p < 0.05$, $^{##}p < 0.01$ for ICH + EXO vs. ICH + Vehicle.
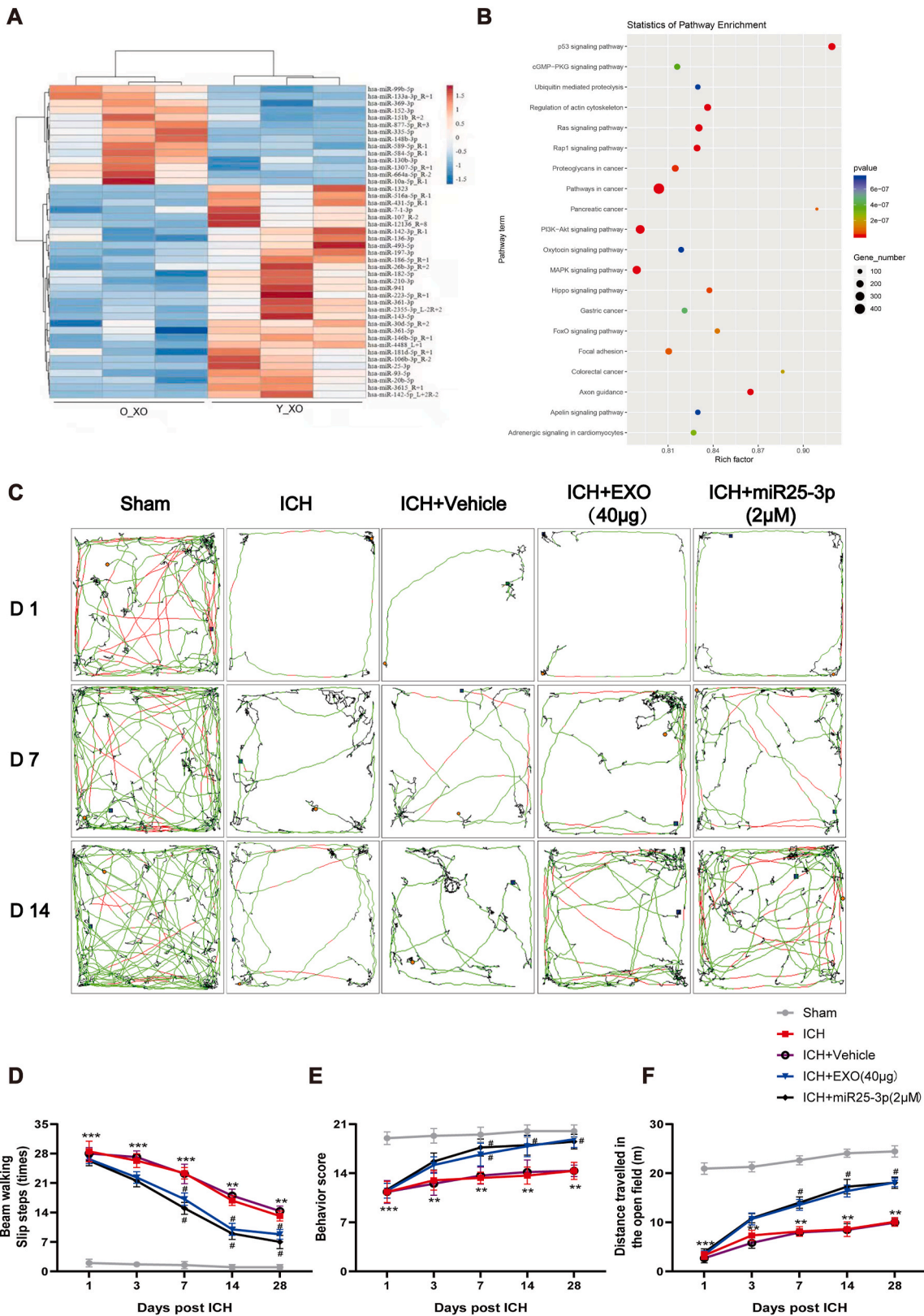
Fig. 5. miR-25-3p mimics the effect of young plasma-derived exosomes on the motor recovery in ICH mice.

(A) Heat map of abundant miRNAs in young and old people plasma derived exosomes by miRNA-seq. (B) The miRNA expression profile of young human plasma-derived exosomes was analyzed, and the target genes of differentially expressed miRNAs in different processes were analyzed by GO. (C) Representative open field movement trajectory of mice in different groups. (D) Beam-walking test showing the slip ratio of the contralateral limbs in different groups. (E) Gross motor function was tested using the modified Garcia behavior score. (F) Summary data showing the distance travelled in the open field from experiments in (C). n = 6 animals for each group, **p < 0.01, ***p < 0.001 for ICH vs. sham; #p < 0.05 for ICH + miR-25-3p or ICH + EXO vs. ICH + Vehicle.

3.6. miR-25-3p mediates the neuroprotective effect of exosomes from young healthy man plasma against ferroptosis after ICH

To further verify whether miR-25-3p treatment could ameliorate ferroptosis after ICH, immunofluorescence staining with GPX4 was performed. The intensity of GPX4 was dramatically diminished in the ICH group compared with the sham group, whereas the exosomes and miR-25-3p robustly suppressed the reduction of GPX4 intensity (Fig. 6A and B). Lipid-peroxidation in the tissue surrounding hematoma was measured using malondialdehyde (MDA) and glutathione (GSH) assays, and most important factors were associated with ferroptosis which were widely reported before. Data showed that GSH was exhausted in day 7 after ICH; however, exosomes or miR-25-3p administration substantially rescued the loss of GSH (Fig. 6C). In contrast, ICH led to pronounced elevation of MDA while both exosomes or miR-25-3p impeded the upregulation of MDA level (Fig. 6D). Furthermore, miR-25-3p inhibitor diminished the effect of exosomes on MDA and GSH. Taken together, these results robustly suggest that hemorrhagic stroke causes elevated lipid peroxidation and decreased anti-oxidation component, thereby inducing ferroptosis in the brain tissue surrounding hematoma, while miR-25-3p, a vital molecule of exosomes, mediates the neuroprotective effect of exosomes against ferroptosis after ICH.
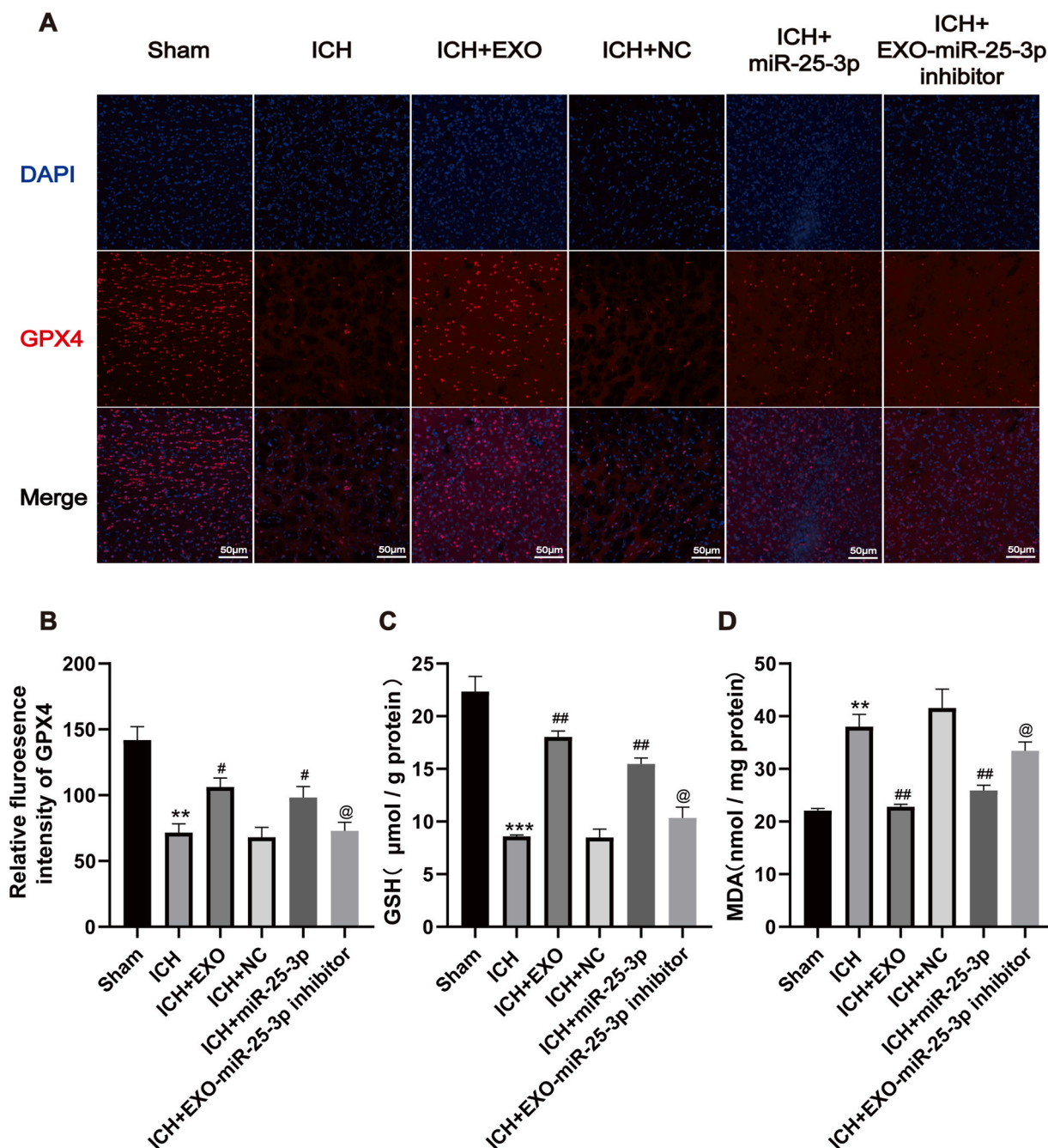

Fig. 6. Young plasma-derived exosomes and miR-25-3p counteract ferroptosis after ICH.
(A) Representative immunofluorescent images of GPX4 around hematoma from different groups. (B) Quantitative analysis of GPX4 staining (Scale bars = 50 μm, n = 4 animals for each group). (C) Quantitative analysis of GSH around hematoma from different groups (n = 5 animals for each group). (D) Quantitative analysis of MDA around hematoma from different groups (n = 5 animals for each group). **$p < 0.01$, ***$p < 0.001$ for ICH vs. sham; #$p < 0.05$, ##$p < 0.01$, for ICH + EXO or ICH + miR-25-3p vs. ICH + EXO-miR-25-3p inhibitor and ICH + NC.

3.7. Exosomes-encapsulated miR-25-3p counteracts ferroptotic injury in response to ICH via regulating P53/SLC7A11/GPX4 pathway

To disclose the underlying mechanism whereby exosomes and miR-25-3p counteract ferroptosis after ICH, PCR and western blotting were firstly employed to observe the changes in SLC7A11 and GPX4 expression. ICH resulted in the downregulation of SLC7A11 and GPX4 at levels of mRNA and protein (Fig. 7A–E). However, exosomes or miR-25-3p reversed the SLC7A11 and GPX4 expression, suggesting that ICH activates ferroptosis through activating SLC7A11/GPX4 pathway [37,38], whereas exosomes or miR-25-3p counteracts this signaling pathway. As aforementioned, RNA-sequence profiling analysis showed that P53 signaling pathway might be associated with miR-25-3p. Thus, we

supposed that P53 might be miR-25-3p′s downstream target [39]. To test this hypothesis, we first used western botting to observe the change of P53 expression after ICH. The data showed increased P53 level in the tissue surrounding hematoma on 7 days after ICH (Fig. 7F and G). After exosomes or miR-25-3p treatment, P53 was down regulated significantly. Second, we used complimentary mRNA sequences to look for possible miR-25-3p targets based on miRbase [40]. The P53 3′UTR matched 6 nucleotides of miR-25-3p 5′UTR (Fig. 7H). We fused the wild-type (WT) and mutated (MUT) sequences of the P53 3′UTR into pGL3-luciferase reporter constructs, and co-transfected the resultant WT or MUT constructs into 293T cells receiving the treatment of miR-25-3p mimic or mimic NC. We observed lower luciferase activity resulting from the P53 3′UTR WT in 293T cells transfected with the miR-25-3p
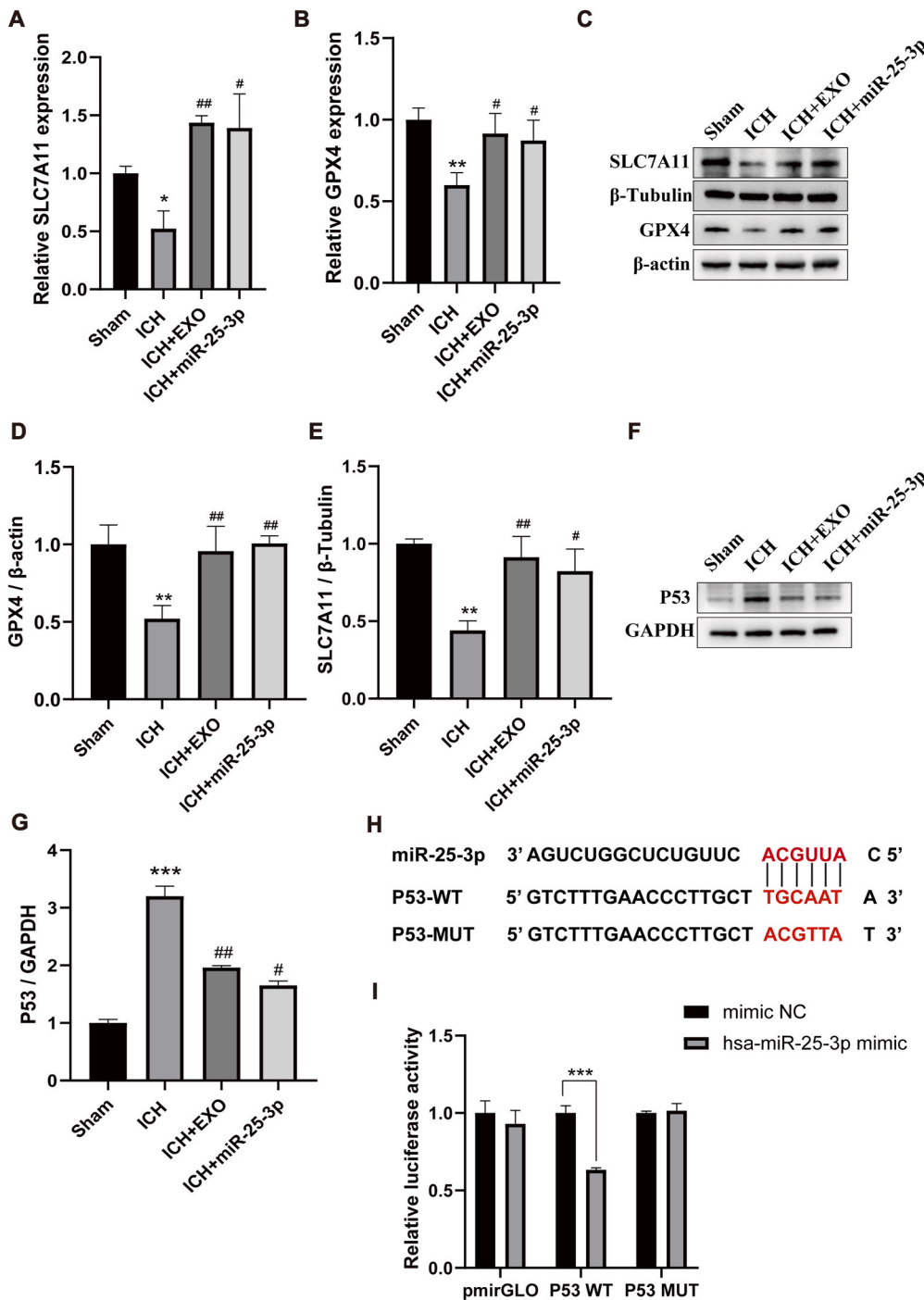

Fig. 7. Exosome-encapsulated miR-25-3p counteracts ferroptotic injury in response to ICH via regulating p53/SLC7A11/GPX4 pathway.

(A–B) Real-time quantitative polymerase chain reaction (qRT-PCR) was used to detect the mRNA expression levels of SLC7A11 and GPX4 around hematoma from different groups (n = 3 animals for each group). (C) Representative Western blotting bands showing the level of SLC7A11 and GPX4 around hematoma from different groups. β-actin and β-Tubulin was served as a loading control. (D–E) Quantitative analysis of GPX4 and SLC7A11 expression level. (F) Representative Western blot of P53 around hematoma from different groups. GAPDH was served as a loading control. (G) Quantitative analysis for the level of P53. n = 6 animals for each group, *p < 0.05, **p < 0.01, ***p < 0.001 for ICH vs. sham; #p < 0.05, ##p < 0.01, for ICH + EXO or ICH + miR-25-3p vs. ICH. (H–I) Luciferase reporter assay demonstrating direct interaction of miR-25-3p with 3′UTR of the P53 gene. One-way ANOVA and Tukey's post hoc test, n = 3, **P < 0.01.

mimics, while no significant change was detected in cells transfected with the mimic NC (Fig. 7I). Therefore, these data suggest that miR-25-3p encapsulated by exosomes counteracts ferroptotic injury by modulating P53/SLC7A11/GPX4 signaling pathway after ICH [41].

4. Discussion

ICH is one of most dreadful brain disease with high mortality and disability. Except intensive antihypertensive therapy [42,43], no available treatment has been proven to be effective for ICH patients. We reported that exosomes from young healthy human plasma could significantly facilitate the functional recovery of ICH mice, whereby miR-25-3p mediates the neuroprotective role by modulating P53/SLC7A11/GPX4 signaling pathway. As far as we know, we are the first to show that exosomes from young healthy man plasma improve functional recovery of ICH, which suggests strong translational potential for the treatment of ICH patients.

If young blood is transferred to the old, rejuvenated, protective and regenerative effects can be generated. Zhang et al. built heterochronic parabiosis models, confirming the hypothesis that juvenile factors can rejuvenate aged systems [44]. Further study showed that cognitive deficits during normal aging can be reversed by exposure to young blood circulation or administration of young blood plasma by improving vascular function, synaptic plasticity and neurogenesis [45,46]. However, we need to clarify the identity or the mechanism of youth-dependent factors with reparative effects in the blood. Youthful circulatory components have been believed to mediate the effect and mechanisms of rejuvenation, regeneration, immunology, and other domains across organ systems [47,48]. It will be interesting to know whether extracellular vesicles including exosomes exert the aforementioned effects of young plasma. This study leveraged the exosomes from young plasma to treat ICH and gained unexpected effect, not only shedding light on the role of exosomes in the potential benefit of young plasma, but also paving a new way for treating hemorrhagic stroke.

Secondary brain injury following ICH plays an essential role in the pathological consequences, such as motor or language disability, paresthesia, and neurological pain. In animal ICH models, ferrous deposition has been found to induce reactive oxygen species (ROS) formation through Fenton reaction, which could cause lipid peroxidation, playing a vital role in ferroptosis [49,50]. Indeed, recent studies have shown pronounced ferroptosis after ICH [51,52]. In this study, we observed increased MDA level and reduced GSH level after ICH. Upregulation of both GPX4 and SLC7A11 was also observed. These data suggest that ferroptotic pathway is activated after ICH.

Exosome is a kind of newly found cellular vesicle that works as a vehicle to deliver message and nutrition through the cell membrane. Exosomes have typical bi-layer membrane structure to make them easily pass through cell membrane. Content inside exosomes was complicated, including RNA sequence, protein and lipid. Apart from nutrient role of exosomes, their signaling transduction role has been gradually figured out [53]. Exosomes are derived from the nanoscale vesicle-like structures of cells with a natural biological origin. Compared with other systems, exosomes are considered one of the most promising drug delivery carriers, due to their selectivity, safety, stability, and long-distance transport of substances. Therefore, exosomes used in the clinical treatment of patients with cerebral hemorrhage is a safe, effective and feasible potential treatment strategy, and its clinical application has a very broad prospect.

Recent years, exosomes derived RNAs, including microRNA, are highly related to signaling transduction. MicroRNAs are noncoding single stranded RNA molecules of about 22 nucleotides long encoded by endogenous genes. It was reported to regulating gene expression at post-transcriptional level. Mechanically, by means of binding with the target mRNA, microRNA could decrease the gene expression by inhibiting translation. Through sequencing, we confirmed that young human plasma-derived exosomes contain abundant miR-25-3p. Previous studies on miR-25-3p have focused on cancer-related biological functions [54,55]. Recent study revealed anti-apoptotic effects of miR-25-3p on cultured primary neurons [56]. However, the association between miR-25-3p and ferroptosis has been less investigated [57], to our best knowledge, this is the first study reveals the effect of miR-25-3p on ICH related ferroptosis.

Similar to apoptosis, ferroptosis, known as programmed cell death, is regulated by a number of pathways [58,59]. SLC7A11-GPX4 pathway is the most typical ferroptosis pathway that was widely studied [60,61]. SLC7A11 is a transmembrane transporter located in intracellular membrane system importing glutamate and exporting cysteine at the same time. Glutamate then inhibits ROS through GPX4, a reduction enzyme inside cell. However, the upstream regulator of SLC7A11 has been less examined. Our results showed that P53 could negatively regulate SLC7A11 expression, suggesting that P53 acts as an upstream regulator of SLC7A11 boosting ferroptosis. Indeed, recent studies [62,63] reported the same results. Furthermore, luciferase assay indicated that miR-25-3p would bind P53 3′UTR to lower its expression at post-transcriptional level. Together, exosomes derived miR-25-3p is an inhibitor of P53 expression and could counteract ferroptotic death from ICH through regulating SLC7A11/GPX4 pathway.

5. Conclusions

In summary, this study demonstrates that exosomes from the plasma of young healthy man enhance functional recovery from ICH via decreasing the injury size and cell death. Mechanistically, exosomes derived miR-25-3p inhibits P53 expression by binding 3′UTR of P53 and then saves the SLC7A11-GPX4 pathway to protect cells from ferroptosis after ICH. To our best knowledge, this is the first work disclosing that exosomes derived from young plasma counteract ferroptosis in ICH through microR-25-3p/P53/SLC7A11/GPX4 axis, which paves a new way to the future treatment of ICH patients.

Ethics approval and consent to participate

Animal Experiments:
All the animal experiments were approved by the Ethics Committee of Southwest Hospital of Third Military Medical University (Chongqing , China; approval no. AMUWEC20224040). All the authors were compliance with all relevant ethical regulations.

Young healthy human plasma obtained:
All the human experiments were approved by the Ethics Committee of Southwest Hospital of Third Military Medical University (Chongqing , China; approval no. AKY2022128). All the authors compliance with all relevant ethical regulations.

CRediT authorship contribution statement

Wenqin Yang: Methodology, Investigation, Formal analysis, Writing – original draft. **Ning Ding:** Investigation, Formal analysis, Writing – review & editing. **Ran Luo:** Investigation, Formal analysis. **Qian Zhang:** Investigation. **Zhenhua Li:** Methodology, Investigation. **Fengchun Zhao:** Investigation. **Shuixian Zhang:** Methodology, Investigation. **Xuyang Zhang:** Investigation. **Tengyuan Zhou:** Investigation. **Haomiao Wang:** Investigation. **Long Wang:** Investigation. **Shengli Hu:** Investigation. **Guixue Wang:** Resources, Funding acquisition. **Hua Feng:** Methodology, Investigation. **Rong Hu:** Conceptualization, Methodology, Writing – original draft, Writing – review & editing, Supervision, Funding acquisition.

Declaration of competing interest

There is no Conflicts of Interest.

Acknowledgments

This work was supported by grants from National Natural Science Foundation of China (81671228), Program for Innovation research group of universities in Chongqing (CXQT19012), Chongqing municipal Science Fund for Distinguished Young Scholars (cstc2019jcyjjqX0030) and Science and Technology Innovation Project of Jinfeng Laboratory, Chongqing, China (jfkyjf202203001).

Appendix A. Supplementary data

Supplementary data to this article can be found online at https://doi.org/10.1016/j.bioactmat.2023.03.007.

References

[1] R.F. Keep, Y. Hua, G.H. Xi, Intracerebral haemorrhage: mechanisms of injury and therapeutic targets, Lancet Neurol. 11 (2012) 720–731, https://doi.org/10.1016/s1474-4422(12)70104-7.

[2] M.Z. Xue, V.W. Yong, Neuroinflammation in intracerebral haemorrhage: immunotherapies with potential for translation, Lancet Neurol. 19 (2020) 1023–1032, https://doi.org/10.1016/s1474-4422(20)30364-1.

[3] R. Hu, C. Zhang, J.S. Xia, H.F. Ge, J. Zhong, X.Y. Fang, Y.J. Zou, C. Lan, L. Li, H. Feng, Long-term outcomes and risk factors related to hydrocephalus after intracerebral hemorrhage, Transl. Stroke Res. 12 (2021) 31–38, https://doi.org/10.1007/s12975-020-00823-y.

[4] J. Aronowski, X.R. Zhao, Molecular pathophysiology of cerebral hemorrhage secondary brain injury, Stroke 42 (2011) 1781–1786, https://doi.org/10.1161/strokeaha.110.596718.

[5] S.J. Dixon, K.M. Lemberg, M.R. Lamprecht, R. Skouta, E.M. Zaitsev, C.E. Gleason, D.N. Patel, A.J. Bauer, A.M. Cantley, W.S. Yang, B. Morrison 3rd, B.R. Stockwell, Ferroptosis: an iron-dependent form of nonapoptotic cell death, Cell 149 (2012) 1060–1072, https://doi.org/10.1016/j.cell.2012.03.042.

[6] L. Zecca, M.B. Youdim, P. Riederer, J.R. Connor, R.R. Crichton, Iron, brain ageing and neurodegenerative disorders, Nat. Rev. Neurosci. 5 (2004) 863–873, https://doi.org/10.1038/nrn1537.

[7] P. Maher, A. Currais, D. Schubert, Using the oxytosis/ferroptosis pathway to understand and treat age-associated neurodegenerative diseases, Cell Chem. Biol. 27 (2020) 1456–1471, https://doi.org/10.1016/j.chembiol.2020.10.010.

[8] B.R. Stockwell, J.P.F. Angeli, H. Bayir, A.I. Bush, M. Conrad, S.J. Dixon, S. Fulda, S. Gascon, S.K. Hatzios, V.E. Kagan, K. Noel, X.J. Jiang, A. Linkermann, M. E. Murphy, M. Overholtzer, A. Oyagi, G.C. Pagnussat, J. Park, Q. Ran, C. S. Rosenfeld, K. Salnikow, D.L. Tang, F.M. Torti, S.V. Torti, S. Toyokuni, K. A. Woerpel, D.D. Zhang, Ferroptosis: a regulated cell death nexus linking metabolism, redox biology, and disease, Cell 171 (2017) 273–285, https://doi.org/10.1016/j.cell.2017.09.021.

[9] X. Yi, X.Q. Tang, Exosomes from miR-19b-3p-modified ADSCs inhibit ferroptosis in intracerebral hemorrhage mice, Front. Cell Dev. Biol. 9 (2021) 11, https://doi.org/10.3389/fcell.2021.661317.

[10] J.R. Wan, H.L. Ren, J. Wang, Iron toxicity, lipid peroxidation and ferroptosis after intracerebral haemorrhage, Stroke Vasc. Neurol. 4 (2019) 93–95, https://doi.org/10.1136/svn-2018-000205.

[11] C. Lu, C. Tan, H. Ouyang, Z. Chen, Z. Yan, M. Zhang, Ferroptosis in intracerebral hemorrhage: a panoramic perspective of the metabolism, mechanism and theranostics, Aging and disease 13 (2022) 1348–1364, https://doi.org/10.14336/ad.2022.01302.

[12] T. Lener, M. Gimona, L. Aigner, V. Borger, E. Buzas, G. Camussi, N. Chaput, D. Chatterjee, F.A. Court, H.A. Del Portillo, L. O'Driscoll, S. Fais, J.M. Falcon-Perez, U. Felderhoff-Mueser, L. Fraile, Y.S. Gho, A. Gorgens, R.C. Gupta, A. Hendrix, D. M. Hermann, A.F. Hill, F. Hochberg, P.A. Horn, D. de Kleijn, L. Kordelas, B. W. Kramer, E.-M. Kramer-Albers, S. Laner-Plamberger, S. Laitinen, T. Leonardi, M. J. Lorenowicz, S.K. Lim, J. Lotvall, C.A. Maguire, A. Marcilla, I. Nazarenko, T. Ochiya, T. Patel, S. Pedersen, G. Pocsfalvi, S. Pluchino, P. Quesenberry, I. G. Reischl, F.J. Rivera, R. Sanzenbacher, K. Schallmoser, I. Slaper-Cortenbach, D. Strunk, T. Tonn, P. Vader, B.W.M. van Balkom, M. Wauben, S.E. Andaloussi, C. Thery, E. Rohde, B. Giebel, Applying extracellular vesicles based therapeutics in clinical trials - an ISEV position paper, J. Extracell. Vesicles 4 (2015) 30087, https://doi.org/10.3402/jev.v4.30087.

[13] L. Cheng, A.F. Hill, Therapeutically harnessing extracellular vesicles, Nat. Rev. Drug Discov. 21 (2022) 379–399, https://doi.org/10.1038/s41573-022-00410-w.

[14] E.J. Bunggulawa, W. Wang, T.Y. Yin, N. Wang, C. Durkan, Y.Z. Wang, G.X. Wang, Recent advancements in the use of exosomes as drug delivery systems, J. Nanobiotechnol. 16 (2018) 13, https://doi.org/10.1186/s12951-018-0403-9.

[15] L.Y. Huang, J.X. Song, H. Cai, P.P. Wang, Q.L. Yin, Y.D. Zhang, J. Chen, M. Li, J. J. Song, Y.L. Wang, L. Luo, W. Wang, S.H. Qi, Healthy serum-derived exosomes improve neurological outcomes and protect blood-brain barrier by inhibiting endothelial cell apoptosis and reversing autophagy-mediated tight junction protein reduction in rat stroke model, Front. Cell. Neurosci. 16 (2022) 14, https://doi.org/10.3389/fncel.2022.841544.

[16] S. Duan, F. Wang, J. Cao, C. Wang, Exosomes derived from MicroRNA-146a-5p-enriched bone marrow mesenchymal stem cells alleviate intracerebral hemorrhage by inhibiting neuronal apoptosis and microglial M1 polarization, Drug Des. Dev. Ther. 14 (2020) 3143–3158, https://doi.org/10.2147/DDDT.S255828.

[17] S. Liu, M. Fan, J.X. Xu, L.J. Yang, C.C. Qi, Q.R. Xia, J.F. Ge, Exosomes derived from bone-marrow mesenchymal stem cells alleviate cognitive decline in AD-like mice by improving BDNF-related neuropathology, J. Neuroinflammation 19 (2022) 35, https://doi.org/10.1186/s12974-022-02393-2.

[18] H. Zhou, Y. He, W. Xiong, S. Jing, X. Duan, Z. Huang, G.S. Nahal, Y. Peng, M. Li, Y. Zhu, Q. Ye, MSC based gene delivery methods and strategies improve the therapeutic efficacy of neurological diseases, Bioact. Mater. 23 (2023) 409–437, https://doi.org/10.1016/j.bioactmat.2022.11.007.

[19] Z.G. Zhang, B. Buller, M. Chopp, Exosomes - beyond stem cells for restorative therapy in stroke and neurological injury, Nat. Rev. Neurol. 15 (2019) 193–203, https://doi.org/10.1038/s41582-018-0126-4.

[20] Y.H. Bei, T. Chen, D.D. Banciu, D. Cretoiu, J.J. Xiao, Circulating exosomes in cardiovascular diseases, in: J. Xiao, S. Cretoiu (Eds.), Exosomes in Cardiovascular Diseases: Biomarkers, Pathological and Therapeutic Effects, 998, Springer-Verlag Singapore Pte Ltd, Singapore, 2017, pp. 255–269.

[21] J.Y. Kang, H. Park, H. Kim, D. Mun, H. Park, N. Yun, B. Joung, Human peripheral blood-derived exosomes for microRNA delivery, Int. J. Mol. Med. 43 (2019) 2319–2328, https://doi.org/10.3892/ijmm.2019.4150.

[22] J. Mair-Jenkins, M. Saavedra-Campos, J.K. Baillie, P. Cleary, F.M. Khaw, W.S. Lim, S. Makki, K.D. Rooney, J.S. Nguyen-Van-Tam, C.R. Beck, Convalescent Plasma Study, G, The effectiveness of convalescent plasma and hyperimmune immunoglobulin for the treatment of severe acute respiratory infections of viral etiology: a systematic review and exploratory meta-analysis, J. Infect. Dis. 211 (2015) 80–90, https://doi.org/10.1093/infdis/jiu396.

[23] W.K. Wang, L.F. Wang, L.H. Ruan, J.Y. Oh, X.W. Dong, Q.C. Zhuge, D.M. Su, Extracellular vesicles extracted from young donor serum attenuate inflammaging via partially rejuvenating aged T-cell immunotolerance, Faseb. J. 32 (2018) 5899–5912, https://doi.org/10.1096/fj.201800059R.

[24] Y.B. Wang, X.J. Zhu, X.M. Jiang, J.W. Guo, Z. Fu, Z. Zhou, P. Yang, H.Y. Guo, X. Guo, G.L. Liang, P. Zeng, G.F. Xiao, J.Z. Ma, X. Yin, L.K. Zhang, C. Yan, C. Y. Zhang, Decreased inhibition of exosomal miRNAs on SARS-CoV-2 replication underlies poor outcomes in elderly people and diabetic patients, Signal Transduct. Targeted Ther. 6 (2021) 9, https://doi.org/10.1038/s41392-021-00716-y.

[25] C. Thery, K.W. Witwer, E. Aikawa, M.J. Alcaraz, J.D. Anderson, R. Andriantsitohaina, A. Antoniou, T. Arab, F. Archer, G.K. Atkin-Smith, D.C. Ayre, J.M. Bach, D. Bachurski, H. Baharvand, L. Balaj, S. Baldacchino, N.N. Bauer, A. A. Baxter, M. Bebawy, C. Beckham, A.B. Zavec, A. Benmoussa, A.C. Berardi, P. Bergese, E. Bielska, C. Blenkiron, S. Bobis-Wozowicz, E. Boilard, W. Boireau, A. Bongiovanni, F.E. Borras, S. Bosch, C.M. Boulanger, X. Breakefield, A.M. Breglio, M.A. Brennan, D.R. Brigstock, A. Brisson, M.L.D. Broekman, J.F. Bromberg, P. Bryl-Gorecka, S. Buch, A.H. Buck, D. Burger, S. Busatto, D. Buschmann, B. Bussolati, E. I. Buzas, J.B. Byrd, G. Camussi, D.R.F. Carter, S. Caruso, L.W. Chamley, Y.T. Chang, C.C. Chen, S. Chen, L. Cheng, A.R. Chin, A. Clayton, S.P. Clerici, A. Cocks, E. Cocucci, R.J. Coffey, A. Cordeiro-da-Silva, Y. Couch, F.A.W. Coumans, B. Coyle, R. Crescitelli, M.F. Criado, C. D'Souza-Schorey, S. Das, A.D. Chaudhuri, P. de Candia, E.F. De Santana, O. De Wever, H.A. del Portillo, T. Demaret, S. Deville, A. Devitt, B. Dhondt, D. Di Vizio, L.C. Dieterich, V. Dolo, A.P.D. Rubio, M. Dominici, M.R. Dourado, T.A.P. Driedonks, F.V. Duarte, H.M. Duncan, R. M. Eichenberger, K. Ekstrom, S.E.L. Andaloussi, C. Elie-Caille, U. Erdbrugger, J. M. Falcon-Perez, F. Fatima, J.E. Fish, M. Flores-Bellver, A. Forsonits, A. Frelet-Barrand, F. Fricke, G. Fuhrmann, S. Gabrielsson, A. Gamez-Valero, C. Gardiner, K. Gartner, R. Gaudin, Y.S. Gho, B. Giebel, C. Gilbert, M. Gimona, I. Giusti, D.C. I. Goberdhan, A. Gorgens, S.M. Gorski, D.W. Greening, J.C. Gross, A. Gualerzi, G. N. Gupta, D. Gustafson, A. Handberg, R.A. Haraszti, P. Harrison, H. Hegyesi, A. Hendrix, A.F. Hill, F.H. Hochberg, K.F. Hoffmann, B. Holder, H. Holthofer, B. Hosseinkhani, G.K. Hu, Y.Y. Huang, V. Huber, S. Hunt, A.G.E. Ibrahim, T. Ikezu, J.M. Inal, M. Isin, A. Ivanova, H.K. Jackson, S. Jacobsen, S.M. Jay, M. Jayachandran, G. Jenster, L.Z. Jiang, S.M. Johnson, J.C. Jones, A. Jong, T. Jovanovic-Talisman, S. Jung, R. Kalluri, S. Kano, S. Kaur, Y. Kawamura, E. T. Keller, D. Khamari, E. Khomyakova, A. Khvorova, P. Kierulf, K.P. Kim, T. Kislinger, M. Klingeborn, D.J. Klinke, M. Kornek, M.M. Kosanovic, A.F. Kovacs, E.M. Kramer-Albers, S. Krasemann, M. Krause, I.V. Kurochkin, G.D. Kusuma, S. Kuypers, S. Laitinen, S.M. Langevin, L.R. Languino, J. Lannigan, C. Lasser, L. C. Laurent, G. Lavieu, E. Lazaro-Ibanez, S. Le Lay, M.S. Lee, Y.X.F. Lee, D.S. Lemos, M. Lenassi, A. Leszczynska, I.T.S. Li, K. Liao, S.F. Libregts, E. Ligeti, R. Lim, S. K. Lim, A. Line, K. Linnemannstons, A. Llorente, C.A. Lombard, M.J. Lorenowicz, A. M. Lorincz, J. Lotvall, J. Lovett, M.C. Lowry, X. Loyer, Q. Lu, B. Lukomska, T. R. Lunavat, S.L.N. Maas, H. Malhi, A. Marcilla, J. Mariani, J. Mariscal, E. S. Martens-Uzunova, L. Martin-Jaular, M.C. Martinez, V.R. Martins, M. Mathieu, S. Mathivanan, M. Maugeri, L.K. McGinnis, M.J. McVey, D.G. Meckes, K.L. Meehan, I. Mertens, V.R. Minciacchi, A. Moller, M.M. Jorgensen, A. Morales-Kastresana, J. Morhayim, F. Mullier, M. Muraca, L. Musante, V. Mussack, D.C. Muth, K. H. Myburgh, T. Najrana, M. Nawaz, I. Nazarenko, P. Nejsum, C. Neri, T. Neri, R. Nieuwland, L. Nimrichter, J.P. Nolan, E.N.M. Nolte-'t Hoen, N. Noren Hooten, L. O'Driscoll, T. O'Grady, A. O'Loghlen, T. Ochiya, M. Olivier, A. Ortiz, L.A. Ortiz, X. Osteikoetxea, O. Ostegaard, M. Ostrowski, J. Park, D.M. Pegtel, H. Peinado, F. Perut, M.W. Pfaffl, D.G. Phinney, B.C.H. Pieters, R.C. Pink, D.S. Pisetsky, E. P. von Strandmann, I. Polakovicova, I.K.H. Poon, B.H. Powell, I. Prada, L. Pulliam, P. Quesenberry, A. Radeghieri, R.L. Raffai, S. Raimondo, J. Rak, M.I. Ramirez, G. Raposo, M.S. Rayyan, N. Regev-Rudzki, F.L. Ricklefs, P.D. Robbins, D. D. Roberts, S.C. Rodrigues, E. Rohde, S. Rome, K.M.A. Rouschop, A. Rughetti, A. E. Russell, P. Saa, S. Sahoo, E. Salas-Huenuleo, C. Sanchez, J.A. Saugstad, M. J. Saul, R.M. Schiffelers, R. Schneider, T.H. Schoyen, A. Scott, E. Shahaj, S. Sharma, O. Shatnyeva, F. Shekari, G.V. Shelke, A.K. Shetty, K. Shiba, P.R.M. Siljander, A.

M. Silva, A. Skowronek, O.L. Snyder, R.P. Soares, B.W. Sodar, C. Soekmadji, J. Sotillo, P.D. Stahl, W. Stoorvogel, S.L. Stott, E.F. Strasser, S. Swift, H. Tahara, M. Tewari, K. Timms, S. Tiwari, R. Tixeira, M. Tkach, W.S. Toh, R. Tomasini, A. C. Torrecilhas, J.P. Tosar, V. Toxavidis, L. Urbanelli, P. Vader, B.W.M. van Balkom, S.G. van der Grein, J. Van Deun, M.J.C. van Herwijnen, K. Van Keuren-Jensen, G. van Niel, M.E. van Royen, A.J. van Wijnen, M.H. Vasconcelos, I.J. Vechetti, T. D. Veit, L.J. Vella, E. Velot, F.J. Verweij, B. Vestad, J.L. Vinas, T. Visnovitz, K. V. Vukman, J. Wahlgren, D.C. Watson, M.H.M. Wauben, A. Weaver, J.P. Webber, V. Weber, A.M. Wehman, D.J. Weiss, J.A. Welsh, S. Wendt, A.M. Wheelock, Z. Wiener, L. Witte, J. Wolfram, A. Xagorari, P. Xander, J. Xu, X.M. Yan, M. Yanez-Mo, H. Yin, Y. Yuana, V. Zappulli, J. Zarubova, V. Zekas, J.Y. Zhang, Z.Z. Zhao, L. Zheng, A.R. Zheutlin, A.M. Zickler, P. Zimmermann, A.M. Zivkovic, D. Zocco, E. K. Zuba-Surma, Minimal information for studies of extracellular vesicles 2018 (MISEV2018): a position statement of the International Society for Extracellular Vesicles and update of the MISEV2014 guidelines, J. Extracell. Vesicles 7 (2018) 43, https://doi.org/10.1080/20013078.2018.1535750.

[26] M.A. Rynkowski, G.H. Kim, R.J. Komotar, M.L. Otten, A.F. Ducruet, B.E. Zacharia, C.P. Kellner, D.K. Hahn, M.B. Merkow, M.C. Garrett, R.M. Starke, B.M. Cho, S. A. Sosunov, E.S. Connolly, A mouse model of intracerebral hemorrhage using autologous blood infusion, Nat. Protoc. 3 (2008) 122–128, https://doi.org/10.1038/nprot.2007.513.

[27] A.-K. Kraeuter, P.C. Guest, Z. Sarnyai, The open field test for measuring locomotor activity and anxiety-like behavior, Methods Mol. Biol. 1916 (2019) 99–103, https://doi.org/10.1007/978-1-4939-8994-2_9.

[28] X.Y. Shi, H.Y. Bai, J.M. Wang, J.R. Wang, L. Huang, M.M. He, X.J. Zheng, Z. T. Duan, D.Y. Chen, J.X. Zhang, X.M. Chen, J. Wang, Behavioral assessment of sensory, motor, emotion, and cognition in rodent models of intracerebral hemorrhage, Front. Neurol. 12 (2021) 17, https://doi.org/10.3389/fneur.2021.667511.

[29] H. Liu, S. He, C. Li, J. Wang, Q. Zou, Y. Liao, R. Chen, Tetrandrine alleviates inflammation and neuron apoptosis in experimental traumatic brain injury by regulating the IRE1alpha/JNK/CHOP signal pathwa, Brain and behavior (2022), e2786, https://doi.org/10.1002/brb3.2786.

[30] J.Y. Hou, G.Z. Cao, L.L. Tian, R. Zhou, Y. Zhang, H. Xu, H.W. Wu, L.F. Wang, H. J. Yang, J.J. Zhang, Integrated transcriptomics and metabolomics analysis reveals that C3 and C5 are vital targets of DuZhi Wan in protecting against cerebral ischemic injury, Biomed. Pharmacother. 155 (2022) 12, https://doi.org/10.1016/j.biopha.2022.113703.

[31] C.J. Li, P. Cheng, M.K. Liang, Y.S. Chen, Q. Lu, J.Y. Wang, Z.Y. Xia, H.D. Zhou, X. Cao, H. Xie, E.Y. Liao, X.H. Luo, MicroRNA-188 regulates age-related switch between osteoblast and adipocyte differentiation, J. Clin. Invest. 125 (2015) 1509–1522, https://doi.org/10.1172/jci77716.

[32] Y. Song, Z. Li, T. He, M. Qu, L. Jiang, W. Li, X. Shi, J. Pan, L. Zhang, Y. Wang, Z. Zhang, Y. Tang, G.Y. Yang, M2 microglia-derived exosomes protect the mouse brain from ischemia-reperfusion injury via exosomal miR-124, Theranostics 9 (2019) 2910–2923, https://doi.org/10.7150/thno.30879.

[33] Y. Kuang, X. Zheng, L. Zhang, X. Ai, V. Venkataramani, E. Kilic, D.M. Hermann, A. Majid, M. Bahr, T.R. Doeppner, Adipose-derived mesenchymal stem cells reduce autophagy in stroke mice by extracellular vesicle transfer of miR-25, J. Extracell. Vesicles 10 (2020), e12024, https://doi.org/10.1002/jev2.12024.

[34] T.M. Seibt, B. Proneth, M. Conrad, Role of GPX4 in ferroptosis and its pharmacological implication, Free Radic. Biol. Med. 133 (2019) 144–152, https://doi.org/10.1016/j.freeradbiomed.2018.09.014.

[35] M. Kumar, Z. Lu, A.A.L. Takwi, W. Chen, N.S. Callander, K.S. Ramos, K.H. Young, Y. Li, Negative regulation of the tumor suppressor p53 gene by microRNAs, Oncogene 30 (2011) 843–853, https://doi.org/10.1038/onc.2010.457.

[36] W. Wan, W. Wan, Y. Long, Q. Li, X. Jin, G. Wan, F. Zhang, Y. Lv, G. Zheng, Z. Li, Y. Zhu, MiR-25-3p promotes malignant phenotypes of retinoblastoma by regulating PTEN/Akt pathway, Biomed. Pharmacother. 118 (2019) 109111, https://doi.org/10.1016/j.biopha.2019.109111.

[37] I. Ingold, C. Berndt, S. Schmitt, S. Doll, G. Poschmann, K. Buday, A. Roveri, X. X. Peng, F.P. Freitas, T. Seibt, L. Mehr, M. Aichler, A. Walch, D. Lamp, M. Jastroch, S. Miyamoto, W. Wurst, F. Ursini, E.S.J. Amer, N. Fradejas-Villar, U. Schweizer, H. Zischka, J.P.F. Angeli, M. Conrad, Selenium utilization by GPX4 is required to prevent hydroperoxide-induced ferroptosis, Cell 172 (2018) 409, https://doi.org/10.1016/j.cell.2017.11.048. -+.

[38] W.S. Yang, R. SriRamaratnam, M.E. Welsch, K. Shimada, R. Skouta, V. S. Viswanathan, J.H. Cheah, P.A. Clemons, A.F. Shamji, C.B. Clish, L.M. Brown, A. W. Girotti, V.W. Cornish, S.L. Schreiber, B.R. Stockwell, Regulation of ferroptotic cancer cell death by GPX4, Cell 156 (2014) 317–331, https://doi.org/10.1016/j.cell.2013.12.010.

[39] L. Jiang, N. Kon, T.Y. Li, S.J. Wang, T. Su, H. Hibshoosh, R. Baer, W. Gu, Ferroptosis as a p53-mediated activity during tumour suppression, Nature 520 (2015) 57, https://doi.org/10.1038/nature14344. +.

[40] A. Kozomara, M. Birgaoanu, S. Griffiths-Jones, miRBase: from microRNA sequences to function, Nucleic Acids Res. 47 (2019) D155–D162, https://doi.org/10.1093/nar/gky1141.

[41] C. Zeng, J. Lin, K.T. Zhang, H.H. Ou, K. Shen, Q.B. Liu, Z.B. Wei, X.H. Dong, X. K. Zeng, L.M. Zeng, W.D. Wang, J. Yao, SHARPIN promotes cell proliferation of cholangiocarcinoma and inhibits ferroptosis via p53/SLC7A11/GPX4 signaling, Cancer Sci. 113 (2022) 3766–3775, https://doi.org/10.1111/cas.15531.

[42] A.I. Qureshi, Y.Y. Palesch, W.G. Barsan, D.F. Hanley, C.Y. Hsu, R.L. Martin, C. S. Moy, R. Silbergleit, T. Steiner, J.I. Suarez, K. Toyoda, Y.J. Wang, H. Yamamoto, B.W. Yoon, A.-T. Investigators, T. Neurological Emergency Treatment, Intensive

[43] C.S. Anderson, E. Heeley, Y. Huang, J. Wang, C. Stapf, C. Delcourt, R. Lindley, T. Robinson, P. Lavados, B. Neal, J. Hata, H. Arima, M. Parsons, Y. Li, J. Wang, S. Heritier, Q. Li, M. Woodward, R.J. Simes, S.M. Davis, J. Chalmers, I. Investigators, Rapid blood-pressure lowering in patients with acute intracerebral hemorrhage, N. Engl. J. Med. 368 (2013) 2355–2365, https://doi.org/10.1056/NEJMoa1214609.

blood-pressure lowering in patients with acute cerebral hemorrhage, N. Engl. J. Med. 375 (2016) 1033–1043, https://doi.org/10.1056/NEJMoa1603460.

[44] W.Q. Zhang, J. Qu, G.H. Liu, J.C.I. Belmonte, The ageing epigenome and its rejuvenation, Nat. Rev. Mol. Cell Biol. 21 (2020) 137–150, https://doi.org/10.1038/s41580-019-0204-5.

[45] S. Ma, S. Wang, Y.X. Ye, J. Ren, R.Q. Chen, W. Li, J.M. Li, L.Y. Zhao, Q. Zhao, G. Q. Sun, Y. Jing, Y.S. Zuo, M.Z. Xiong, Y.H. Yang, Q.R. Wang, J.H. Lei, S.H. Sun, X. Long, M.S. Song, S.Y. Yu, P. Chan, J.W. Wang, Q. Zhou, J.C.I. Belmonte, J. Qu, W.Q. Zhang, G.H. Liu, Heterochronic parabiosis induces stem cell revitalization and systemic rejuvenation across aged tissues, Cell Stem Cell 29 (2022) 990, https://doi.org/10.1016/j.stem.2022.04.017. -+.

[46] L. Katsimpardi, N.K. Litterman, P.A. Schein, C.M. Miller, F.S. Loffredo, G. R. Wojtkiewicz, J.W. Chen, R.T. Lee, A.J. Wagers, L.L. Rubin, Vascular and neurogenic rejuvenation of the aging mouse brain by young systemic factors, Science 344 (2014) 630–634, https://doi.org/10.1126/science.1251141.

[47] I.M. Conboy, M.J. Conboy, A.J. Wagers, E.R. Girma, I.L. Weissman, T.A. Rando, Rejuvenation of aged progenitor cells by exposure to a young systemic environment, Nature 433 (2005) 760–764, https://doi.org/10.1038/nature03260.

[48] S.A. Villeda, K.E. Plambeck, J. Middeldorp, J.M. Castellano, K.I. Mosher, J. Luo, L. K. Smith, G. Bieri, K. Lin, D. Berdnik, R. Wabl, J. Udeochu, E.G. Wheatley, B. D. Zou, D.A. Simmons, X.M.S. Xie, F.M. Longo, T. Wyss-Coray, Young blood reverses age-related impairments in cognitive function and synaptic plasticity in mice, Nat. Med. 20 (2014) 659–663, https://doi.org/10.1038/nm.3569.

[49] L. Magtanong, S.J. Dixon, Ferroptosis and brain injury, Dev. Neurosci. 40 (2019) 382–395, https://doi.org/10.1159/000496922.

[50] Y. Zhang, S. Khan, Y. Liu, R.Y. Zhang, H.M. Li, G.F. Wu, Z.P. Tang, M.Z. Xue, V. W. Yong, Modes of brain cell death following intracerebral hemorrhage, Front. Cell. Neurosci. 16 (2022) 15, https://doi.org/10.3389/fncel.2022.799753.

[51] X.Y. Wang, T. Mori, T. Sumii, E.H. Lo, Hemoglobin-induced cytotoxicity in rat cerebral cortical neurons - caspase activation and oxidative stress, Stroke 33 (2002) 1882–1888, https://doi.org/10.1161/01.Str.0000020121.41527.5d.

[52] G.H. Xi, R.F. Keep, J.T. Hoff, Mechanisms of brain injury after intracerebral haemorrhage, Lancet Neurol. 5 (2006) 53–63, https://doi.org/10.1016/s1474-4422(05)70283-0.

[53] A. Thakur, D.C. Parra, P. Motallebnejad, M. Brocchi, H.J. Chen, Exosomes: small vesicles with big roles in cancer, vaccine development, and therapeutics, Bioact. Mater. 10 (2022) 281–294, https://doi.org/10.1016/j.bioactmat.2021.08.029.

[54] Z.C. Zeng, Y.L. Li, Y.J. Pan, X.L. Lan, F.Y. Song, J.B. Sun, K. Zhou, X.L. Liu, X. L. Ren, F.F. Wang, J.L. Hu, X.H. Zhu, W. Yang, W.T. Liao, G.X. Li, Y.Q. Ding, L. Liang, Cancer-derived exosomal miR-25-3p promotes pre-metastatic niche formation by inducing vascular permeability and angiogenesis, Nat. Commun. 9 (2018) 14, https://doi.org/10.1038/s41467-018-07810-w.

[55] B.Q. Chen, Y. Zhao, Y. Zhang, Y.J. Pan, H.Y. Xia, R.K. Kankala, S.B. Wang, G. Liu, A.Z. Chen, Immune-regulating camouflaged nanoplatforms: a promising strategy to improve cancer nano-immunotherapy, Bioact. Mater. 21 (2023) 1–19, https://doi.org/10.1016/j.bioactmat.2022.07.023.

[56] R. Li, Y.T. Wen, B. Wu, M.Q. He, P. Zhang, Q.B. Zhang, Y.M. Chen, MicroRNA-25-3p suppresses epileptiform discharges through inhibiting oxidative stress and apoptosis via targeting OXSR1 in neurons, Biochem. Biophys. Res. Commun. 523 (2020) 859–866, https://doi.org/10.1016/j.bbrc.2020.01.050.

[57] X.K. Jiang, S.Q. Guo, M.Y. Xu, B.J. Ma, R.L. Liu, Y. Xu, Y.Y. Zhang, TFAP2C-Mediated lncRNA PCAT1 inhibits ferroptosis in docetaxel-resistant prostate cancer through c-Myc/miR-25-3p/SLC7A11 signaling, Front. Oncol. 12 (2022) 18, https://doi.org/10.3389/fonc.2022.862015.

[58] K. Bersuker, J.M. Hendricks, Z. Li, L. Magtanong, B. Ford, P.H. Tang, M.A. Roberts, B. Tong, T.J. Maimone, R. Zoncu, M.C. Bassik, D.K. Nomura, S.J. Dixon, J. A. Olzmann, The CoQ oxidoreductase FSP1 acts parallel to GPX4 to inhibit ferroptosis, Nature 575 (2019) 688–692, https://doi.org/10.1038/s41586-019-1705-2.

[59] C. Mao, X. Liu, Y. Zhang, G. Lei, Y. Yan, H. Lee, P. Koppula, S. Wu, L. Zhuang, B. Fang, M.V. Poyurovsky, K. Olszewski, B. Gan, DHODH-mediated ferroptosis defence is a targetable vulnerability in cancer, Nature 593 (2021) 586–590, https://doi.org/10.1038/s41586-021-03539-7.

[60] X. Liu, C. Chen, D. Han, W. Zhou, Y. Cui, X. Tang, C. Xiao, Y. Wang, Y. Gao, SLC7A11/GPX4 inactivation-mediated ferroptosis contributes to the pathogenesis of triptolide-induced cardiotoxicity, Oxid. Med. Cell. Longev. 2022 (2022), 3192607, https://doi.org/10.1155/2022/3192607.

[61] X. Guan, Z. Li, S. Zhu, M. Cheng, Y. Ju, L. Ren, G. Yang, D. Min, Galangin attenuated cerebral ischemia-reperfusion injury by inhibition of ferroptosis through activating the SLC7A11/GPX4 axis in gerbils, Life Sci. 264 (2021), 118660, https://doi.org/10.1016/j.lfs.2020.118660.

[62] Y. Luo, X. Gao, L. Zou, M. Lei, J. Feng, Z. Hu, Bavachin induces ferroptosis through the STAT3/P53/slc7a11 Axis in osteosarcoma cells, Oxid. Med. Cell. Longev. 2021 (2021), 1783485, https://doi.org/10.1155/2021/1783485.

[63] S. Ma, L. Sun, W. Wu, J. Wu, Z. Sun, J. Ren, USP22 protects against myocardial ischemia-reperfusion injury via the SIRT1-p53/slc7a11-dependent inhibition of ferroptosis-induced cardiomyocyte death, Front. Physiol. 11 (2020), 551318, https://doi.org/10.3389/fphys.2020.551318.